Development & Experimental Assessment of Robust Direction Finding and Self-Calibration

Christian C. Jones[1], Zeus E. Gannon[1], Dan DePardo[1], Jonathan W. Owen[1], Shannon D. Blunt[1], Christopher T. Allen[1], Benjamin H. Kirk[2]
[1]Radar Systems Lab (RSL), University of Kansas (KU), Lawrence, KS
[2]U.S. Army Research Laboratory (ARL), Adelphi, MD

***Abstract*—The reiterative super-resolution (RISR) algorithm was developed to perform adaptive direction finding while accounting for model errors from imperfect calibration. Here this approach is extended to incorporate additional model error attributes and a self-calibration formulation is likewise developed that can exploit illuminators of opportunity. Efficacy of the overall method is experimentally demonstrated using open-air measurements from an 8-element uniform linear array (ULA), an ad hoc 4×4 planar array, and a 4-element ULA streamed by an RF-SoC.**

Keywords—array processing, direction finding, array calibration, spatial isolation

I. Introduction

Direction finding (DF) is an application of array processing that involves determining the relative direction of arrival of signals impinging on an antenna array. With increasing congestion of the radio frequency (RF) spectrum [1], subsequent growing demands on cognitive operation [2], and the expectation of increasing dependence on space-division multiple access (SDMA) [3], there is need to perform DF efficiently and accurately in a manner that is robust to the physical environment and practical system fidelity limitations.

Classical adaptive DF methods rely on collection of time snapshots of the RF environment to construct a sample covariance matrix (SCM), then employ the SCM inverse or subspaces of the SCM. The minimum variance distortionless response (MVDR) [4] is an example of the former and multiple signal classification (MUSIC) [5] is an example of the latter, with numerous variations thereof and other related methods [6].

Where SCM approaches impose a stationarity requirement and also necessitate methods such as spatial smoothing to address spatio-temporal coupling from multipath [7], we instead leverage a structured covariance matrix. For spatial processing this form is denoted as RISR [8, 9], a repurposing of reiterative minimum mean-square error (RMMSE) estimation originally developed for adaptive pulse compression in radar [10], though numerous variants and applications have since been realized and experimentally validated (e.g. [11-14]).

A key attribute of RISR as developed in [9] is the incorporation of a tolerance term for model mismatch that takes the form of multiplicative error, thereby seeking to account for the fact that perfect calibration is not possible in practice. Here this perspective is expanded to address mutual coupling and the higher sensitivity that arises from phase errors, ultimately leading to a self-calibration approach inspired by [15] that realizes a calibrated array manifold by bootstrapping from an initial idealized manifold and observed signals of opportunity. Doing so also involves leveraging a "partial constraint" form of RISR [16] that facilitates additional robustness in practice.

Here it is experimentally demonstrated that DF can be performed with a single snapshot, though noncoherent combining of a few snapshots provides further enhancement up to a point. Consequently, exquisite time granularity can be achieved. Results are shown for an 8-channel uniform linear array (ULA) and a 4×4 quasi-uniform planar array, both relying on high-speed oscilloscopes for data capture, in addition to a 4-channel ULA using an RF system-on-a-chip (RF-SoC) for streaming data capture. Moreover, the practical spatial isolation of signals demonstrated here enables further enhanced time-domain processing that is explored in the companion paper [17].

II. Robust Direction Finding

The idealized single-snapshot linear model for an arbitrary array manifold with N elements can be represented as

$$\mathbf{y}(\ell) = \mathbf{S}\,\mathbf{x}(\ell) + \mathbf{v}(\ell)\,, \tag{1}$$

where ℓ denotes the discrete time index, $\mathbf{S}$ is an $N \times M$ matrix of spatial steering vectors (with $M >> N$), the $M \times 1$ vector $\mathbf{x}(\ell)$ contains instantaneous complex amplitudes of incident signals corresponding to the steering vectors in $\mathbf{S}$, and $\mathbf{v}(\ell)$ is an $N \times 1$ vector of additive noise across the array. The actual number of signals present K is generally limited to be less than M, though recent efforts have shown how the co-array can be exploited to combat this limitation (e.g. [18, 19]). Rank estimation is also commonly employed to supplement the estimation of $\mathbf{x}(\ell)$ [20], though is unnecessary for RISR and may hinder self-calibration.

The idealized model in (1) neglects physical reality in which imperfect calibration in the form inexact element positions and beampatterns, mutual coupling, and RF channel gain/phase/timing errors can significantly degrade performance. We can compensate this model (to some degree) by extending the model mismatch perspective in [9], so that (1) becomes

$$\begin{aligned}\mathbf{y}(\ell) &= [\tilde{\mathbf{S}}\,\mathbf{x}(\ell)] \odot \mathbf{z} + \mathbf{v}(\ell) \\ &= [\tilde{\mathbf{S}}\,\mathbf{x}(\ell)] + \mathbf{v}(\ell) + \mathbf{v}_{\mathrm{z}}(\ell)\,,\end{aligned} \tag{2}$$

with

$$\mathbf{v}_{\mathrm{z}}(\ell) = (\mathbf{z} - \mathbf{1}_{N\times 1}) \odot [\tilde{\mathbf{S}}\,\mathbf{x}(\ell)] \tag{3}$$

and

$$\tilde{\mathbf{S}} = \mathbf{C}\,(\mathbf{S} \odot \mathbf{Q}) \tag{4}$$

incorporates uncertainties and mutual coupling. Specifically, the nth element of $N \times 1$ vector $\mathbf{z}$ in (2) and (3) is modeled as [9]

$$z_n = [1 + \Delta_{\mathrm{a},n}]\,e^{j\Delta_{\varphi,n}}\,, \tag{6}$$

This work was supported by the Army Research Office under Grant #W911NF-20-2-0271. DISTRIBUTION STATEMENT A. Approved for Public Release.

where $\Delta_{a,n}$ and $\Delta_{\varphi,n}$ are real-valued independent random variables accounting for general amplitude and phase errors, respectively. The (n, m) term in $N \times M$ matrix $\mathbf{Q}$ is modeled as

$$q_{n,m} = \exp\{j2\pi\, u_n \sin(\phi_m)\} \tag{7}$$

to also include element position uncertainty (for a ULA), with u_n and ϕ_n likewise real-valued independent random variables. Finally,

$$\mathbf{C} = \mathbf{T}\,\mathbf{F} \tag{8}$$

accounts for mutual coupling, where $\mathbf{T}$ is a complex and symmetric (not Hermitian) Toeplitz matrix and $\mathbf{F}$ is a diagonal matrix of mutual coupling gains [15, 21, 22]. In practice (8) is not perfectly known and can vary with spatial angle, with errors also inducing deviation from the assumed Teoplitz × diagonal matrix structure. Consequently, we shall refine an estimate of $\mathbf{C}$ iteratively in conjunction with RISR DF operation, thereby reducing model error to an achievable tolerance.

The optimized $N \times M$ bank of RMMSE filters $\mathbf{W}(\ell)$ can be obtained by minimizing

$$J = E\{\|\mathbf{x}(\ell) - \mathbf{W}^H(\ell)\mathbf{y}(\ell)\|^2\} \tag{9}$$

for $E\{\bullet\}$ denoting expectation. Differentiating (9) with respect to $\mathbf{W}(\ell)$, equating to zeros and solving, then incorporating the compensated model from (2) and associated statistical properties yields the mth compensated DF filter

$$\mathbf{w}_m(\ell) = \mathbf{G}_{m,m}\,\mathbf{P}_{m,m}(\ell)\left[\mathbf{R}_{\text{S-D}}(\ell) + \mathbf{R}_{\text{S-OD}}(\ell) + \mathbf{R}_{\text{v}}\right]^{-1}\widehat{\mathbf{C}}\mathbf{s}_m\,. \tag{10}$$

Here $\mathbf{R}_{\text{v}}$ is the noise covariance, $\widehat{\mathbf{C}}$ is the current estimate of (8), and $\mathbf{s}_m$ is the mth column of steering vector matrix $\mathbf{S}$. We have decomposed the structured covariance matrix $\mathbf{R}_{\text{S}}(\ell) = \mathbf{R}_{\text{S-D}}(\ell) + \mathbf{R}_{\text{S-OD}}(\ell)$ into a diagonal component

$$\mathbf{R}_{\text{S-D}}(\ell) = \left(\widehat{\mathbf{C}}\,\mathbf{S}\,\mathbf{P}(\ell)\mathbf{S}^H\widehat{\mathbf{C}}^H\right) \odot \left[\left(1+\sigma_z^2\right)\mathbf{I}_{N\times N}\right] \tag{11}$$

and an off-diagonal component

$$\mathbf{R}_{\text{S-OD}}(\ell) = \left(\widehat{\mathbf{C}}\mathbf{S}\,\mathbf{G}\,\mathbf{P}(\ell)\mathbf{G}^H\mathbf{S}^H\widehat{\mathbf{C}}^H\right) \odot \left(\mathbf{1}_{N\times N} - \mathbf{I}_{N\times N}\right), \tag{12}$$

where

$$\mathbf{P}(\ell) = E\{\mathbf{x}(\ell)\,\mathbf{x}^H(\ell)\} \tag{13}$$

is the spatial power density (diagonal by enforcing independence), with $\mathbf{P}_{m,m}(\ell)$ in (10) the mth diagonal term, σ_z^2 is the general gain/phase uncertainty variance of (6), and $\mathbf{G}$ is a diagonal position-uncertainty weighting matrix (for ULAs) resulting from $\mathbf{Q}$ in which the (m, m) term is

$$\mathbf{G}_{m,m} = \exp\left\{-\frac{1}{2}\left(2\pi\sin(\phi_m)\right)^2\sigma_u^2\right\} \tag{14}$$

for σ_{u}^2 the variance in element position.

In practice, $\mathbf{P}(\ell)$ from (13) is not known *a priori*, but can be estimated for the ith iteration via

$$\hat{\mathbf{P}}_i(\ell) = \left[\frac{1}{2L+1}\sum_{\Delta\ell=-L}^{L}\hat{\mathbf{x}}_{i-1}(\ell+\Delta\ell)\,\hat{\mathbf{x}}_{i-1}^H(\ell+\Delta\ell)\right] \odot \mathbf{I}_{M\times M} \tag{15}$$

where

$$\hat{\mathbf{x}}_i(\ell) = \mathbf{W}_i^H(\ell)\,\mathbf{y}(\ell) \tag{16}$$

is the ith complex amplitude estimate across the M spatial directions for the ℓth snapshot, which is obtained by applying the ith filter bank $\mathbf{W}_i(\ell) = [\mathbf{w}_{1,i}(\ell)\ \ \mathbf{w}_{2,i}(\ell)\ \cdots\ \mathbf{w}_{M,i}(\ell)]$. This process is initialized by setting $\mathbf{W}_{i=0}(\ell) = \mathbf{S}$, with the RISR portion then applying (15), (10), and (16) for i = 1, 2, …, I_{iter} iterations. Setting L = 0 for (15) enables estimation on a single-snapshot basis, though increasing L to 10 or so provides considerable improvement due to (noncoherent) averaging.

It was shown in [16] that a gain-constrained form of RISR can be readily obtained, which avoids possible suppression of low SNR signals that can occur in the unconstrained version. A related outcome of the gain-constrained form is preservation of the noise floor, which is also useful for meaningful detection relative to a background response. The one drawback to this form is less super-resolution enhancement.

In the interest of obtaining a "best of breed", [16] combined these two versions into a "partially constrained" (PC) form, which in this compensated model context realizes

$$\mathbf{w}_{\text{PC},m}(\ell) = \left[\left(\frac{1}{\mathbf{s}_m^H\,\mathbf{D}(\ell)\,\mathbf{s}_m}\right)^{\alpha}\left(\mathbf{G}_{m,m}\,\mathbf{P}_{m,m}(\ell)\right)^{1-\alpha}\right]\mathbf{D}(\ell)\widehat{\mathbf{C}}\mathbf{s}_m \tag{17}$$

where

$$\mathbf{D}(\ell) = \left[\mathbf{R}_{\text{S-D}}(\ell) + \mathbf{R}_{\text{S-OD}}(\ell) + \mathbf{R}_{\text{v}}\right]^{-1} \tag{18}$$

is the inverted matrix from (10) and α is the partial constraint term that can be tuned to fully gain-constrained $(\alpha = 1)$ or fully unconstrained $(\alpha = 0)$. Values between these extremes provide a useful trade-space to prevent small signal suppression, enhance robustness, and improve spatial separability. The combination of this partial constraint form and the various uncertainty/tolerance terms also enables greater flexibility to establish practical operating regimes.

III. RISR Self-Calibration

Regardless of the DF approach employed, inaccurate array calibration leads to poor performance. However, the iterative implementation of RISR, combined with the compensated modeling discussed above, facilitates the means with which to bootstrap improved calibration using signals of opportunity.

Inspired by [15], consider the least squares cost function

$$J_{\text{cal}} = \left\|\mathbf{y}(\ell) - \widehat{\mathbf{C}}\left(\mathbf{S}\,\mathbf{G}\right)\hat{\mathbf{x}}(\ell)\right\|^2 \tag{19}$$

which assesses the error between the measured snapshot $\mathbf{y}(\ell)$ and the expected measurement based on the given spatial estimate $\hat{\mathbf{x}}(\ell)$, the $\mathbf{C}$ estimate, $\mathbf{S}$, and $\mathbf{G}$. While (19) does not have a closed form solution, descent methods (here quasi-Newton) can be used to update $\widehat{\mathbf{C}}$ so that model error is minimized. Of course, a poor initial estimate of $\hat{\mathbf{x}}(\ell)$ in (19) can propagate bias and errors in $\widehat{\mathbf{C}}$. To combat this effect, an iterative self-calibration routine is proposed that leverages RISR model uncertainty and the partial constraint.

Specifically, self-calibration is enabled by first performing RISR using $\widehat{\mathbf{C}} = \mathbf{I}$ (or with calibration measurements if known), α set to be small (< 0.5), and large model uncertainty $(\sigma_{\text{u}}^2 > 1)$. This parameter combination emphasizes dominant signal components and suppresses lower power signals. The estimate $\widehat{\mathbf{C}}$ is subsequently refined with the new $\hat{\mathbf{x}}(\ell)$ estimate, σ_{u}^2 is reduced, and RISR is repeated. This loop is performed until convergence or after sufficient reduction in σ_{u}^2 is acheived. A depiction of this approach is shown in Fig. 1. While not required, the use of multiple snapshots and known calibration sources can improve solution quality. Alternatively, this method could be applied “on the fly” where the calibration is updated on an as-needed basis using observed signals.

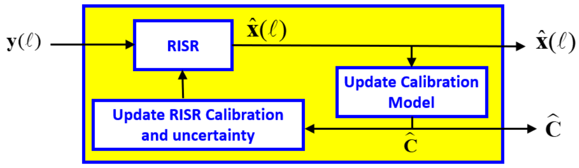

Fig. 1. Block diagram of RISR self-calibration

IV. Open-Air Experimental Validation

To demonstrate this practical instantiation of adaptive DF, three different experimental arrangements were employed. Two of these use high-fidelity test equipment, in linear and planar array configurations, while the third uses an RF-SoC to likewise show progress toward real-time implementation.

A. N = 8 element ULA captured by 8-channel oscilloscope

Consider the arrangement in Fig. 2, where an 8-channel Tektronix MSO68B oscilloscope was used for receive capture of concurrent signals produced by three transmitters. Both transmitters (Tx) and receivers (Rx) used log-periodic antennas with 2-11 GHz bandwidth. This test was conducted with $\lambda/2$ spacing corresponding to 3.95 GHz (selected because it is the given spacing between receive ports in Fig. 2), realizing a 22.5° Rayleigh resolution. No array mount or prior calibration was performed, so self-calibration was critical. The geometry resulted in actual receive directions of −33.7°, −18.4°, and 0° for Tx 1 through Tx 3, respectively. Each transmitter was driven by an arbitrary waveform generator (AWG) producing unique signals in the same band. Due to different amplification, Tx 2 was produced at roughly 10 dB higher power than Tx 1 or 3, though all three emitted on the order of milliwatts. Ambient background noise was collected when the three transmitters were not emitting to estimate the noise covariance.

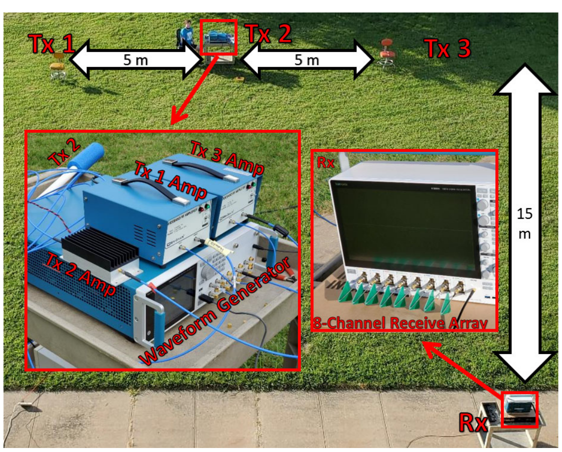

Fig. 2. Open-air experimental setup for DF with 8-channel ULA

The emitted signals comprise an OFDM signal with 500 subcarriers having 100% duty cycle (Tx 1); a linear FM (LFM) radar waveform with 88% duty cycle and 12.5 μs pulse duration (Tx2); and a random FM (RFM) waveform having a Gaussian power spectrum, 66% duty-cycle, and 17.5 μs pulse duration. These very high duty cycles are clearly not typical, but were used to emulate more stressing scenarios with multiple signals while still including the transient on/off behavior. The three signals share the same 10 MHz bandwidth centered at 3.82 GHz, thus realizing a congested and time-varying scenario.

Direction finding was first performed without calibration to establish a performance baseline. Figs. 3-6 depict DF estimates over time for a nonadaptive beamformer (i.e. $\mathbf{S}^H \mathbf{y}(\ell)$) that is Taylor windowed, MVDR using 15 snapshots, and uncalibrated RISR with both 1 and 15 snapshots, respectively. Here RISR was implemented with $M = 160$, $I_{\text{iter}} = 30$ iterations, $\alpha = 0.45$, $\sigma_z^2 = 10^{-3}$, and $\sigma_u^2 = 5 \times 10^{-3}$. Clearly, the lack of calibration has produced multiple false signals and blurred responses across all methods, with the enhanced dynamic range and super-resolution capability of RISR revealing more of this detail for both the single and 15 snapshot cases.

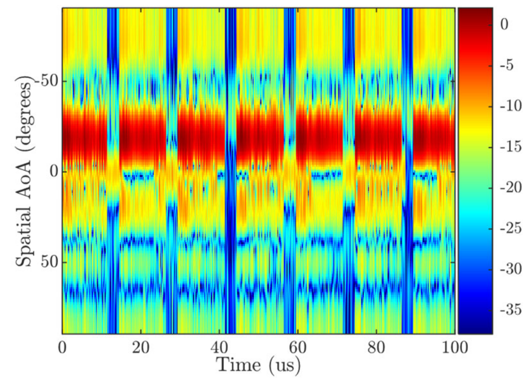

Fig. 3. Nonadaptive beamformer for *N* = 8 ULA (uncalibrated)

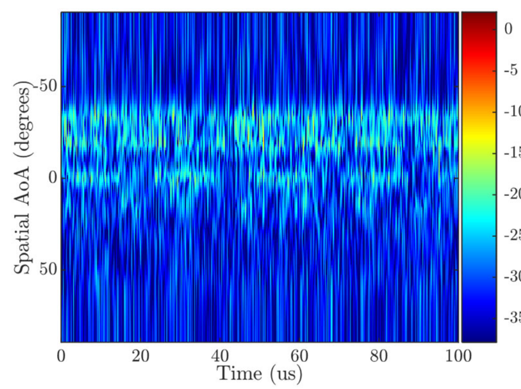

Fig. 4. MVDR beamformer for *N* = 8 ULA, 15 snapshots (uncalibrated)

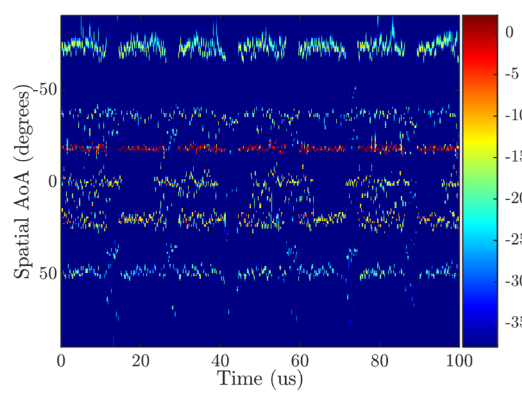

Fig. 5. RISR beamformer for *N* = 8 ULA, 1 snapshot (uncalibrated)

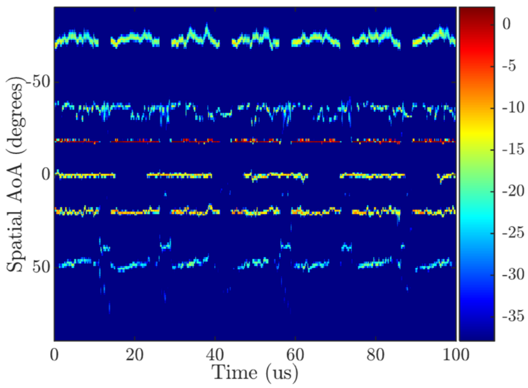

Fig. 6. RISR beamformer for $N = 8$ ULA, 15 snapshots (uncalibrated)

An "on-the-fly" calibration was performed using the approach described in Sect. III with no prior knowledge of emitters or their received directions. At 5 μs intervals the calibration model was updated based on the previous RISR DF estimates until convergence was achieved. Model uncertainty was initialized to $\sigma_z^2 = 1$ and reduced every 5 μs until reaching $\sigma_z^2 = 10^{-3}$. With this large uncertainty, RISR ignores low-power signals because they appear to be multiplicative error artifacts induced by the combination of high-power signals and model errors. The subsequent reduction of uncertainty as calibration estimation is refined permits the DF capture of these smaller signals.

For both single and 15 snapshot RISR implementations, the calibration matrix converges after 75 μs. Figs. 7-10 again show DF estimates over time for nonadaptive, MVDR, and the two RISR implementations, albeit now with the self-calibration routine engaged from the beginning. The most significant improvement is observed in all four figures after the first 5 μs interval, with the 15-snapshot RISR case realizing a very precise determination of signal spatial angles. Note that the upper response in each plot is the lower-power OFDM signal that also possesses significant amplitude modulation. While quite visible after 20 μs of self-calibration by RISR in Fig. 10, it is rather blurry in the single-snapshot RISR (Fig. 9) and MVDR (Fig. 8) results, and completely lost in the nonadaptive case (Fig. 7). Fig. 9 is thereby notable in the degree of accuracy that can actually be obtained when operating on only a single snapshot at a time, though there is clearly a benefit to using more (i.e. Fig. 10).

Fig. 11 provides a root mean-square (RMS) DF response after calibration has completed to assess the accuracy of each angle estimate. We see that the three adaptive approaches produce accurate angle estimates for the LFM and RFM signals, though each has a ~2° error for the OFDM signal, which could well be due to inaccuracies in the test setup. In terms of detectability, 15-snapshot RISR offers 2-3 dB improvement over MVDR for the lower power signals, while the 1-snapshot version incurs degradation relative to MVDR. Further utility of these results in terms of signal characterization after spatial isolation is examined in the companion paper [17].

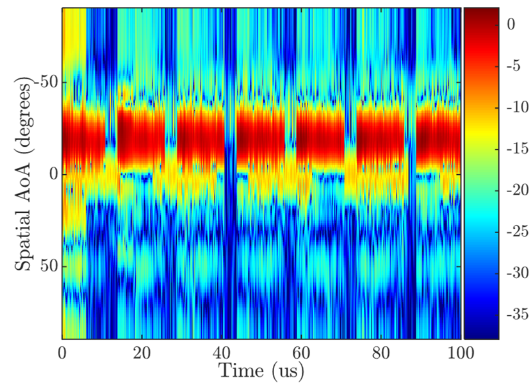

Fig. 7. Nonadaptive beamformer for $N = 8$ ULA (calibrating)

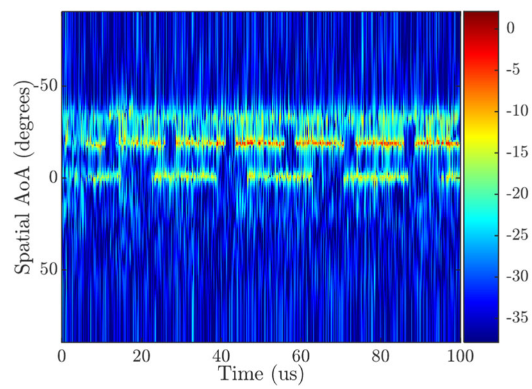

Fig. 8. MVDR beamformer for $N = 8$ ULA, 15 snapshots (calibrating)

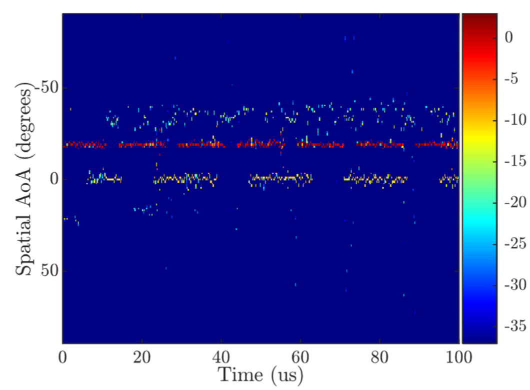

Fig. 9. RISR beamformer for $N = 8$ ULA, 1 snapshot (calibrating)

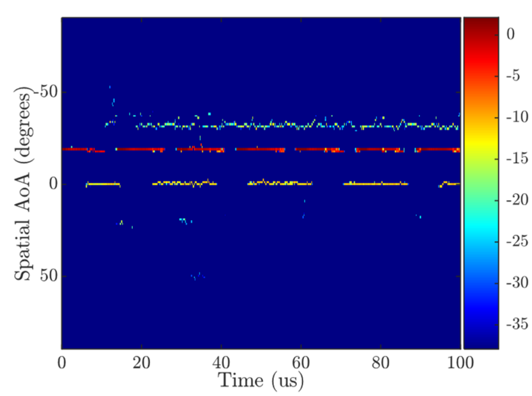

Fig. 10. RISR beamformer for $N = 8$ ULA, 15 snapshots (calibrating)

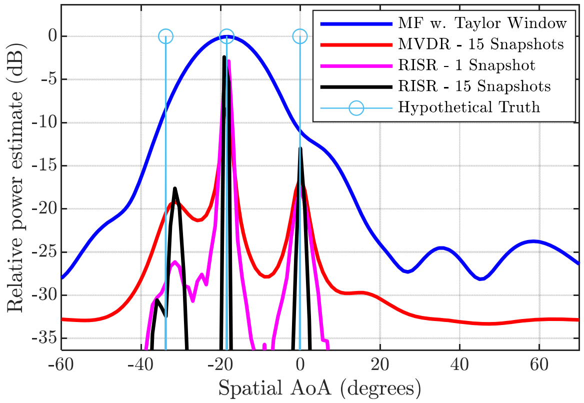

Fig. 11. RMS DF estimates after calibration $N = 8$ ULA

B. $N = 4$ element ULA captured by RF-SoC

To provide further assessment of RISR DF and self-calibration, Dr. Ben Kirk at the U.S. Army Research Lab performed an independent collection using 4 channels of an RF-SoC for data capture, which was calibrated using RISR beforehand, with $\lambda/2$ spacing corresponding to 3.75 GHz. Here an LTE uplink emitter at 3.71 GHz was placed at +15.9° and range of 21.8 feet, and a CW tone at 3.708 GHz was generated from an emitter at −12.3° and range of 20.0 feet.

Parameterizing RISR with $M = 160$, $I_{\text{iter}} = 20$ iterations, $\alpha = 0.45$, $\sigma_z^2 = 10^{-2}$, and $\sigma_u^2 = 5 \times 10^{-2}$, Fig. 12 depicts the DF estimates over time after calibration and using 9 snapshots. Once again, the amplitude modulation of OFDM produces a more variable response in the lower trace (positive angle), while the CW tone is rather constant, albeit with a small degree of estimation variation. That said, both signals are quite clearly isolated spatially, thus enabling further signal characterization (e.g. via [17]).

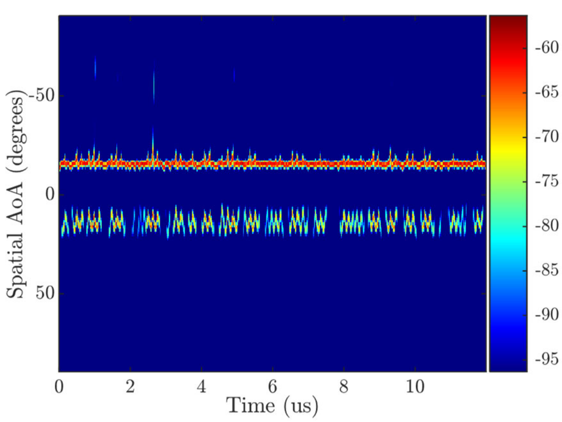

Fig. 12. RISR beamformer for $N = 4$ RF-SoC ULA, 9 snapshots (after calibration)

C. 4×4 planar array via two 8-channel oscilloscopes

Finally, in the interest of demonstrating the extension of this methodology to a two-dimensional "planar" arrangement, the rather ad hoc array depicted in Fig. 13 was "constructed". The reader will note that the elements are not equally spaced, nor do the tilt angles of the elements align very well. Each element is fed directly into one of the receive ports of the two synchronized 8-channel oscilloscopes that are likewise shown. Our intent for this haphazard arrangement was to demonstrate the capability of RISR self-calibration to overcome limitations in fidelity caused by model error, since deviation from the ideal array manifold would most certainly be expected here. Indeed, as an homage we refer to this configuration as a "Van Trees array", both because his well-known book is used as crude element spacing and because the pages within advocate the benefits of optimized receive processing, as demonstrated here.

Fig. 13. Benchtop experimental setup for DF with 4×4 "Van Trees array"

The nominal separation of elements in the horizontal and vertical directions corresponds to $\lambda/2$ spacing at ~2.75 GHz. An indoor open-air test was conducted using three emitters at different azimuths and elevations. In this case a single signal at boresight (with prior angle knowledge) and distance of 10m was first used to perform RISR calibration. The two additional emitters were then switched on, both at about −10° elevation and about ±6° in azimuth, significantly less than the nominal beamwidth in either dimension.

The boresight signal in this case was a 3.82 GHz CW tone while the other two emitters used the same 3.82 GHz RFM signal and LFM waveform as in Sect. IV.A. Here we examine a 25 μs collect, process with 33 snapshots (L=16), and $M = 10{,}000$ steering vectors uniformly spaced in azimuth and elevation (i.e. 100 × 100). The RISR DF implementation also used $I_{\text{iter}} = 30$ iterations, $\alpha = 0.45$, $\sigma_z^2 = 10^{-2}$, and $\sigma_u^2 = 0.5$ since array manifold uncertainty is rather higher than before.

An RMS azimuth-elevation response is plotted for the nonadaptive (Taylor windowed) beamformer, MVDR, and RISR in Figs. 14-16. Both the nonadaptive and MVDR responses smear the lower elevation signals together, with only the former possibly identifying the boresight signal (with some bias). The MVDR response has particularly poor dynamic range. The RISR response, in contrast, clearly identifies the 3 signals, albeit with a similar bias to the boresight signal, which may signify the limit to which calibration could be achieved. The presence of what looks to be a smaller fourth and fifth signal could also be a calibration artifact, or possibly multipath since the indoor environment had many possible reflection surfaces. The key take away is that, despite the rather ad hoc array in Fig. 13, a reasonable DF response could still be obtained by this calibrating form of RISR, suggesting a useful degree of practical robustness.

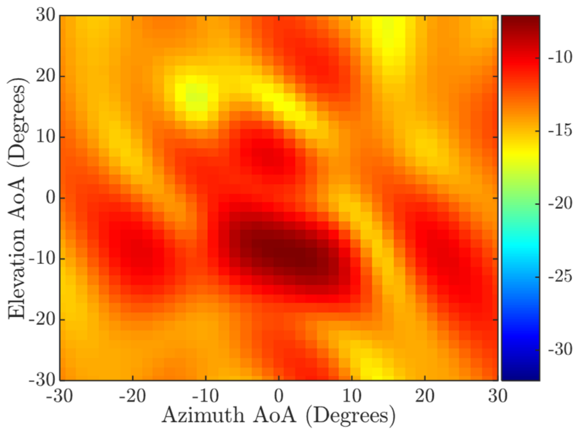

Fig. 14. Nonadaptive beamformer for 4 × 4 array (calibrated)

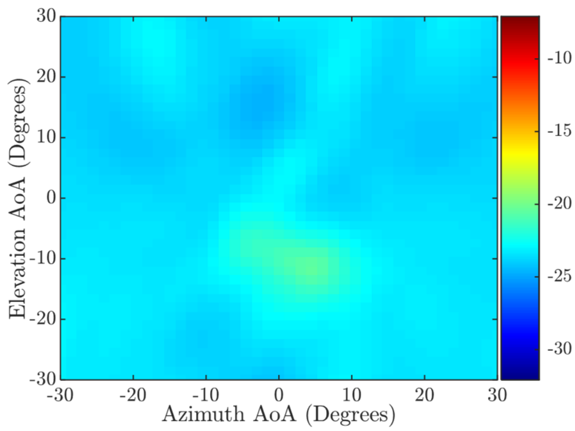

Fig. 15. MVDR beamformer for 4 × 4 array (calibrated)

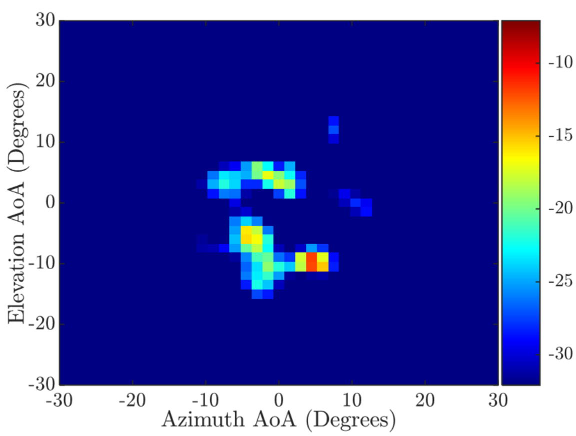

Fig. 15. RISR beamformer for 4 × 4 array (calibrated)

V. Conclusions

The reiterative super-resolution (RISR) algorithm has been shown via three distinct experimental arrangements to provide a robust direction-finding capability that achieves super-resolution and enhances dynamic range. Moreover, a self-calibration process is readily incorporated that can be performed "on the fly" using signals of opportunity or known signals. The resulting spatial isolation facilitates subsequent processing to realize improved signal characterization, which is demonstrated in the companion paper [17].

References

[1] H. Griffiths, L. Cohen, S. Watts, E. Mokole, C. Baker, M. Wicks, S. Blunt, "Radar spectrum engineering and management: technical and regulatory issues," *Proc. IEEE*, vol. 103, no. 1, pp. 85-102, Jan. 2015.

[2] A.F. Martone, et al., "Closing the loop on cognitive radar for spectrum sharing," *IEEE Aerospace & Electronic Systems Mag*., vol. 36, no. 9, pp. 44-55, Sept. 2021.

[3] S.V. Bana, P. Varaiya, "Space division multiple access (SDMA) for robust ad hoc vehicle communication networks," *IEEE Intelligent Transportation Systems*, Oakland, CA, Aug. 2001.

[4] S. Haykin, *Adaptive Filter Theory*, Prentice-Hall, 2002.

[5] R. Schmidt, "Multiple emitter location and signal parameter estimation," *IEEE Trans. Antennas & Prop.*, vol. 34, no. 3, pp. 276-280, Mar. 1986.

[6] H.L. Van Trees, *Optimum Array Processing: Part IV of Detection, Estimation, and Modulation Theory*, John Wiley & Sons, Inc., 2002.

[7] T. Shan, M. Wax, T. Kailath, "On spatial smoothing for direction-of-arrival estimation of coherent signals," *IEEE Trans. Acoustics Speech & Signal Processing*, vol. ASSP-33, no. 4, pp. 806-844, Aug. 1985.

[8] S.D. Blunt, T. Chan, K. Gerlach, "A new framework for direction-of-arrival estimation," *IEEE Sensor Array & Multichannel Signal Processing Workshop*, Darmstadt, Germany, July 2008.

[9] S.D. Blunt, T. Chan, K. Gerlach, "Robust DOA estimation: the reiterative superresolution (RISR) algorithm," *IEEE Trans. Aerospace and Electronic Systems*, vol. 47, no. 1, pp. 332-346, Jan. 2011.

[10] S.D. Blunt, K. Gerlach, "Adaptive pulse compression via MMSE estimation," *IEEE Trans. Aerospace & Electronic Systems*, vol. 42, no. 2, pp. 572-584, July 2006.

[11] D. Henke, P. McCormick, S.D. Blunt, T. Higgins, "Practical aspects of optimal mismatch filtering and adaptive pulse compression for FM waveforms," IEEE Intl. Radar Conf., Washington, DC, May 2015.

[12] P.M. McCormick, S.D. Blunt, "Shared-spectrum multistatic radar: experimental demonstration using FM waveforms," *IEEE Radar Conf.*, Oklahoma City, OK, Apr. 2018.

[13] C.C. Jones, L.A. Harnett, C.A. Mohr, S.D. Blunt, C.T. Allen, "Structure-based adaptive radar processing for joint clutter cancellation and moving target estimation," IEEE Intl. Radar Conf., Washington, DC, Apr. 2020.

[14] L.A. Harnett, B. Ravenscroft, S.D. Blunt, C.T. Allen, "Experimental evaluation of adaptive Doppler estimation for PRI-staggered radar," IEEE Radar Conf., New York City, NY, Mar. 2022.

[15] B.D. Cordill, S.A. Seguin, S.D. Blunt, "Mutual coupling calibration using the Reiterative Superresolution (RISR) algorithm," *IEEE Radar Conf.*, Cincinnati, OH, May 2014.

[16] E. Hornberger, S.D. Blunt, T. Higgins, "Partially constrained adaptive beamforming for super-resolution at low SNR," *IEEE Intl. Workshop Computational Advances in Multi-Sensor Adaptive Processing,* Cancun, Mexico, Dec. 2015.

[17] C.C. Jones, Z.E. Gannon, S.D. Blunt, C.T. Allen, A.F. Martone, "An adaptive spectrogram estimator to enhance signal characterization" *IEEE Radar Conf*., New York City, NY, Mar. 2022.

[18] K.R. Mills, E. Aboutanios, F. Ahmad, "Iterative interpolated beam-forming for exploiting full degrees-of-freedom in DOA estimation with co-prime arrays," *IEEE Intl. Workshop on Computational Advances in Multi-Sensor Adaptive Processing*, Le gosier, Guadeloupe, Dec. 2019.

[19] H.F. Alqadah, D.P. Scholnik, "A reiterative superresolution approach for direction of arrival estimation with sparse arrays," *IEEE Radar Conf.*, Oklahoma City, OK, Apr. 2018.

[20] P. Chen, T.-J. Wu, J. Yang, "A comparative study of model selection criteria for the number of signals," *IET Radar, Sonar & Navigation*, vol. 2, no. 3, pp. 180-188, 2008.

[21] W. Chen, J.P. Lie, B.P. Ng, T. Wang, M.H. Er, "Joint gain/phase and mutual coupling array calibration technique with single calibrating source," *Intl. J. Antennas & Propagation*, Article ID 625165, 2012.

[22] B. Friedlander, A.J. Weiss, "Direction finding in the presence of mutual coupling," *IEEE Trans. Antennas & Propagation*, vol. 39, no. 3, pp. 273-284, Mar. 1991.